INŽENÝRSKÁ MECHANIKA 2005
NÁRODNÍ KONFERENCE
s mezinárodní účastí
Svratka, Česká republika, 9. - 12. května 2005

APPLICATION OF FINITE VOLUME METHOD TO FREE SURFACE FLOW

B. Hoření*, Z. Chára*

Summary: *The contribution deals with an application of discontinuous Galerkin method to free surface flow calculation. Both the super- and sub-critical flows are studied for steady and unsteady flow conditions. The numerical method is tested experimentally on flow over a broad crest weir of height to length ratio 1/8. Also VOF (volume of fluid) method is tested for the same geometrical configuration.*

1. Introduction

Free surface flow, mainly flood propagation, still possesses a great deal of concern. During last decade, an enormous amount of work on mathematical modelling has been done. There are two major groups of mathematical approach to handle the free surface flow. The first one is well known Navier-Stokes equations or some simplifications of them like Reynolds-Averaging-Navier-Stokes equations (RANS), LES and others. The free surface is moving with the velocity of the fluid particles located at the boundary and therefore its position is one of the unknowns and has to be solved by an additional numerical method. VOF (volume of fluid) is a possibility how to include free surface problem to numerical procedures. The second mathematical approach simplifying the solution is a depth averaging procedure of the N-S equations that leads to Shallow Water Equations. In our contribution we focus on the application of a finite volume method to solve the one-dimensional SWE by means of discontinuous Galerkin method. Also an example of CFD modelling of steady flow over an obstacle is presented.

2. Unsteady channel flow

On the beginning let we consider a usual assumption of hydrostatic pressure distribution in the channel. Such assumption results in a neglect of the vertical acceleration component. Integrating of momentum conservation equations over a channel area the classical equations of the open channel flow can be derived. The resulting equations of mass and momentum conservations of the one-dimensional unsteady channel flow of arbitrary cross section are as follows

* Ing. Bohumír Hoření, CSc., Ing. Zdeněk Chára, CSc.: Institute of Hydrodynamics AS CR; Pod Paťankou 30/5, 166 12 Praha 6; tel.: + 420.233323748, fax: + 420.233324361; e-mail: chara@ih.cas.cz

$$\frac{\partial \boldsymbol{Q}}{\partial t} + \frac{\partial \boldsymbol{F}}{\partial x} = \boldsymbol{S}, \tag{1}$$

where vectors of variables $\boldsymbol{Q}$, fluxes $\boldsymbol{F}$ and source terms $\boldsymbol{S}$ are given as (Tseng, 1999)

$$\boldsymbol{Q} = \begin{pmatrix} A \\ Q \end{pmatrix}, \quad \boldsymbol{F} = \begin{pmatrix} Q \\ Q^2/A + gI_1 \end{pmatrix}, \tag{2}$$

$$\boldsymbol{S} = \begin{pmatrix} q_e \\ gI_2 + gA(S_o - S_f) + q_e v_{ex} \end{pmatrix}, \tag{3}$$

where A is local cross section area, Q is flow discharge, g is acceleration of gravity, $S_0 = -\mathrm{d}z/\mathrm{d}x$ is channel bed slope, $q_e[m^3 s^{-1} m^{-1}]$ is intensity of external flow discharge, v_{ex} is velocity component of external source in x direction.

Influence of hydrostatic pressure distribution I_1 and pressure force acting due to the variation of the channel width I_2 can be written as

$$I_1 = \int_0^{h(x,t)} (h-\eta)\, b\,(x,\eta)\, \mathrm{d}\eta\,, \quad I_2 = \int_0^{h(x,t)} (h-\eta)\, \frac{\partial\, b\,(x,\eta)}{\partial x}\, \mathrm{d}\eta, \tag{4}$$

where $b(x,\eta) = \partial A(x,\eta)/\partial\eta$ and h is flow depth (Fig. 1). For trapezoidal cross section (and as special case also for rectangular and triangular cross section) the integrals I_1 and I_2 have the analytical form

$$I_1 = h^2 \left(\frac{B}{2} + \frac{h\,\sigma}{3}\right), \tag{5}$$

$$I_2 = h^2 \left(\frac{1}{2}\frac{\mathrm{d}B}{\mathrm{d}x} + \frac{h}{3}\frac{\mathrm{d}\,\sigma}{\mathrm{d}x}\right), \tag{6}$$

where B is width of channel bed and σ is side slope $(1 : \sigma)$

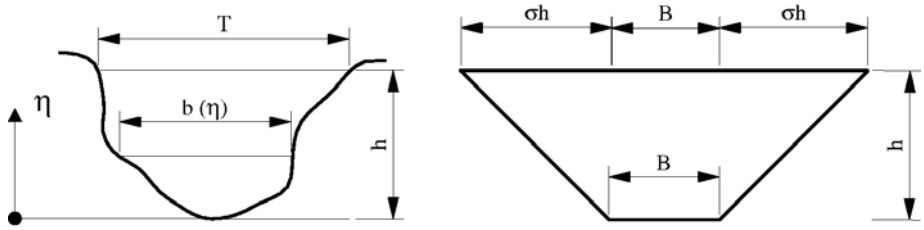

Fig. 1 Channel cross section

The friction slope S_f is given by the following equation

$$S_f = \frac{Q|Q|}{A^2 C^2 R}, \tag{7}$$

where $R = A/O$ is hydraulic radius defined as ratio of cross sectional area of flow, A, to wetted perimeter ratio, O. Velocity or "Chezy" coefficient C $[\mathrm{m}^{0.5}\,\mathrm{s}^{-1}]$ incorporates an influence of viscosity. A lot of empirical or semi-empirical relations of the velocity coefficient can be found. For example Pavlovsky suggested following form

$$C = \frac{R^P}{n}, \quad P = 2.5\sqrt{n} - 0.13 - 0.75\sqrt{R}\,(\sqrt{n} - 0.1), \tag{8}$$

where n is related with bed roughness (generally with channel condition). Another somewhat simpler relation is well known Manning's equation

$$C = \frac{R^{1/6}}{n}. \tag{9}$$

Above derived partially empirical equations are able to solve a number of real problems with sufficient accuracy. For the channel of infinite width, precisely for unit section, it is possible to use flow depth h instead of flow area A and flow discharge Q can be replaced by $h\overline{v}$ where $\overline{v}$ is mean velocity. The result is following set of vector equations (without external sources)

$$\boldsymbol{Q} = \begin{pmatrix} h \\ h\overline{v} \end{pmatrix}, \quad \boldsymbol{F} = \begin{pmatrix} h\overline{v} \\ h\overline{v}^2 + gh^2/2 \end{pmatrix}, \tag{10}$$

$$\boldsymbol{S} = \begin{pmatrix} 0 \\ gh(S_o - S_f) \end{pmatrix}. \tag{11}$$

This form is known as shallow water equations and can be derived directly from general equations by the classical Saint-Vennant approach (de Saint-Vennant, 1871).

3. Numerical procedure

The conservative equations were solved with help of the discontinuous Galerkin method of first order (Hulsen, 1991, Atkins & Shu, 1998). This method originates from classical methods of finite volumes (LeVeque, 2002) but it assumes that inside the elements the searching functions are approximated by functions of higher orders. Individual elements mutually communicate via fluxes through element boundaries. On the boundaries we permit a function discontinuity and we handle with them by a similar manner as in classical methods of finite volumes.

Let us consider an element V bounded by a surface S with outer normal $\boldsymbol{n}$. Inside the element the problem can be described via balance of quantity ϕ in the following form

$$\frac{\partial \phi}{\partial t} + \frac{\partial (\phi v_i)}{\partial x_i} - \sigma \equiv \frac{\partial \phi}{\partial t} + \operatorname{div}(\phi \boldsymbol{v}) - \sigma \equiv \frac{\partial \phi}{\partial t} + \nabla \circ (\phi \boldsymbol{v}) - \sigma = 0 \tag{12}$$

where $\boldsymbol{v}$ if flow velocity and σ is production of ϕ in unit volume. The product of ϕ and $\boldsymbol{v}$ can be considered as flux $\boldsymbol{F}$

$$\boldsymbol{F} = \phi \boldsymbol{v}, \quad F_i = \phi v_i. \tag{13}$$

Let us choose a basis of linearly independent functions φ_i with finite number of members N. Basis φ_i has to be completed in the space of dimension d. If we set the order of the highest member as m then $N = N(m, d)$. Additionally we suppose an approximate solution of ϕ inside the element in the form of linear combination of basis functions

$$\phi \approx \sum_{j=1}^{N} c_j \varphi_j. \tag{14}$$

Complete discretization contains basis of both the spatial and the time functions. But there is a possibility to divide only space on the elements. The basis then contains functions of positional vectors and the coefficients c_j depending on the time. The problem results in a solution of ordinary differential equations for $c_j(t)$.

If we put the approximate solution back to the initial equations, the sum of all elements is not exactly zero, but it equals a value ε.

$$\varepsilon = \sum_{j=1}^{N} \frac{\partial c_j}{\partial t} \varphi_j + \sum_{j=1}^{N} \operatorname{div}\,(c_j \varphi_j \boldsymbol{v}) - \sigma. \tag{15}$$

Galerkin method supposes that the error ε is orthogonal to all basis functions. Corresponding scalar products of functions φ_k and ε have to be zero

$$\int_V \varphi_k \, \varepsilon \, \mathrm{d}V = 0 \quad \text{for} \quad k = 1 \ldots N. \tag{16}$$

In comparison with other methods requesting zero value of error ε in selected points of the element, Galerkin method uses an integral condition in the whole domain V.

These conditions have to be satisfied for all elements of function basis ($k = 1 \ldots N$). Set of equations for unknown values of derivations $\partial c_j / \partial t$ can be written in matrix form. Let us introduce scalar $\mathsf{c} = [c_0, c_1 \ldots c_N]^T$, matrix $\mathsf{M}(N, N)$, with scalar elements

$$m_{kj} = \int_V \varphi_k \, \varphi_j \, \mathrm{d}V, \tag{17}$$

and vectors $\mathsf{g}, \mathsf{a}, \mathsf{s}$ which elements are given as

$$\begin{aligned} g_k &= \int_V \mathbf{grad}\ \varphi_k \circ \boldsymbol{F} \, \mathrm{d}V, \\ a_k &= \int_S \varphi_k \, \boldsymbol{F} \circ \boldsymbol{n} \, \mathrm{d}S, \\ s_k &= \int_V \varphi_k \, \sigma \, \mathrm{d}V. \end{aligned} \tag{18}$$

Then the time derivation of vectors of coefficients c could be rewritten in the form

$$\mathsf{M} \frac{\partial \mathsf{c}}{\mathrm{d}\, t} = \mathsf{g}(\mathsf{c}) - \mathsf{a}(\mathsf{c}) + \mathsf{s}(\mathsf{c}). \tag{19}$$

If the basis functions φ_j are properly chosen the matrix M can gain more suitable forms (for example if the basis functions φ_j are orthogonal the result is a diagonal matrix M, for orthonormal functions φ_j the result is an unit matrix M).

A numerical solution is presented based on the Runge–Kutta method (Gottlieb & Shu, 1998, Gottlieb et al., 2001). To obtain stability a slope limiter is applied on every computational result of the Runge–Kutta method.

4. Experimental set-up

The above presented numerical approach was compared with experimental observations. As a flow situation a simple flow over a broad crest weir has been chosen. The experiments were conducted in a hydraulic flume of square cross section 0.25x0.25 m and of length 6 m. Both the side-walls and the channel bottom are made from smooth glass tables. The broad crest weir of trapezoidal cross section was placed 4 m from the channel inlet. Schematic view of the geometrical arrangement is shown in Fig. 2. Height of the weir was 30 mm, length 240 mm on the top and 300 mm on the channel bed. The slope of the channel bed was set to zero.

The shape of free surface over the weir was visualized by a digital video camera and the individual frames were subsequently processed on PC. The flow depths were continuously monitored with help of an ultrasound sensor Pepperl-Fuchs UC500-30GM-V1. Flow rates were measured by an inductive flow meter Krohne located on a delivery pipe. Due to the pump capacity the maximum attainable flow discharge was slightly below 10 l/sec. The flow discharges were controlled via a turncock situated just downstream the pump. Both the flow depths and flow rates were simultaneously handled on PC via PCMCIA card National Instrument with frequency of 20Hz.

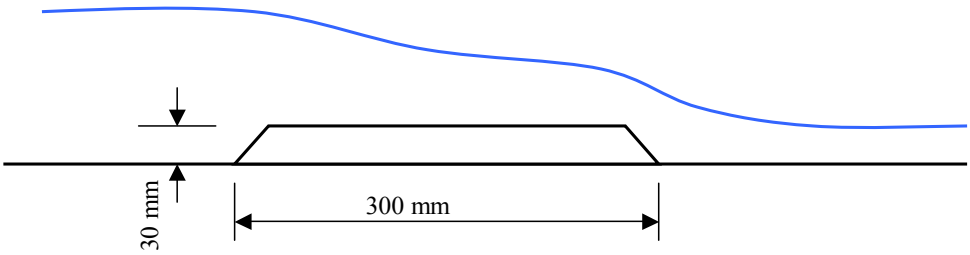

Fig. 2 Schematic view of the broad crest weir

5. CFD modelling

Together with experimental observations and solution of shallow water equations also a CFD calculation of flow over the broad crest weir was performed. By means of Fluent 6.1 the standard two-dimensional k-ε model and the volume of fluid model solving the free surface were adopted. The VOF model is a surface-tracking technique applied to a fixed Eulerian mesh. It is designed for two or more immiscible fluids where the position of the interface between the fluids is of interest. In the VOF model, a single set of momentum equations is shared by the fluids, and the volume fraction of each of the fluids in each computational cell is tracked throughout the domain.

In the case of interest the solution domain was 2.5 m long and 0,25 m height. To accelerate the numerical procedure and quickly balance an amount of liquid and air phases the laminar model was used on beginning. After that the solver was switched to the standard k-ε model performing unsteady flow calculation with time step of 0.001 sec.

6. Results and discussion

6.1. Steady flow condition

During the steady flow measurements the flow rates were kept constant and after stabilising both the flow depths upstream and downstream the weir were monitored. Also the shapes of free surface over the weir were picked up by the digital video camera. Besides the experimental observation the numerical simulations were tested. Shallow water equations solved by the Galerkin method of first order were applied on a mesh of grid size 5 mm. A value *n=0.01* was chosen as the Maning's roughness parameter. The CFD modelling was tested only for one flow rate due to an enormous demand of computational time.

Fig. 3 shows the measured and computed flow depths for various flow discharges. The results proved the correctness of numerical simulations in the regions where the vertical acceleration can be neglected. As concern the free surface over the weir the situation is somewhat different. The assumption of negligible vertical acceleration is no more valid mainly at the end of the weir and the result of numerical simulation is far from the experimental data. The profiles of free surface over the weir are shown in Fig. 4. The numerical simulation quickly achieves the critical flow condition while the real data get to critical condition near the end of the weir.

Fig. 5 shows the CFD results (Fluent) of free surface profile for the flow discharge Q= 8.7 l/sec. CFD solution is very close to the experimental data over the first half of the weir. But at the end of the weir the CFD data underestimate the real data, probably due to the poor simulation of the vortex region just downstream the upper edge of the weir. This is documented in Fig. 6 where the flow visualization is compared with the vectors of velocity field.

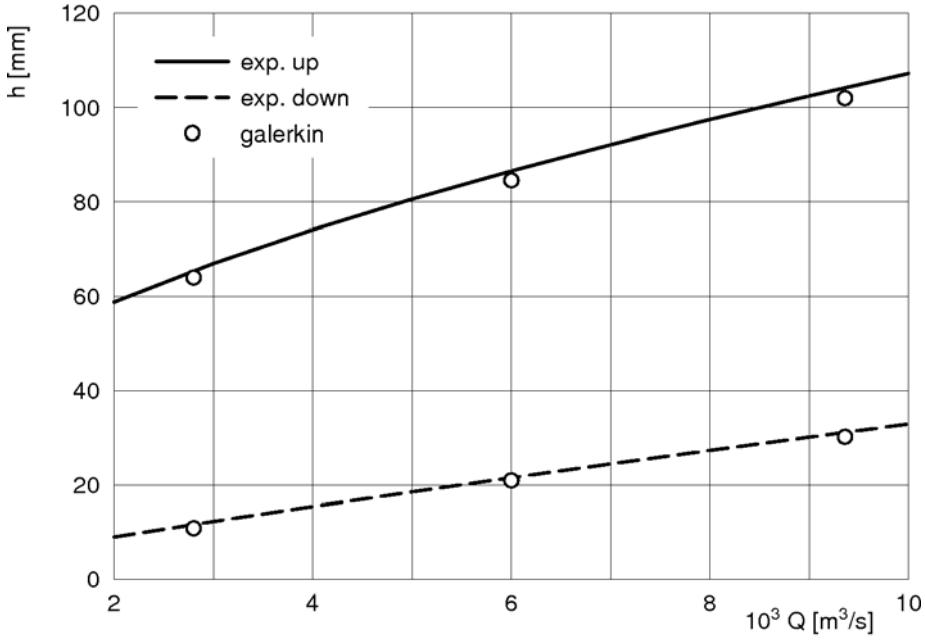

Fig. 3 Sub- and super-critical steady flow conditions upstream and downstream the crest weir

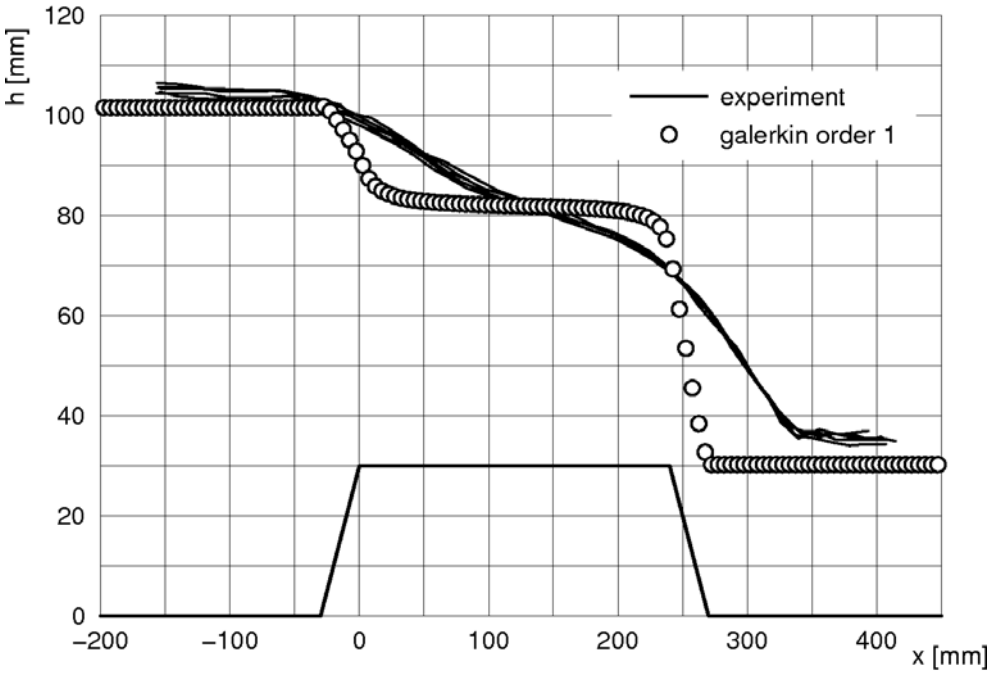

Fig. 4 Free surface profiles over the crest weir (Q=9.4 l/sec)

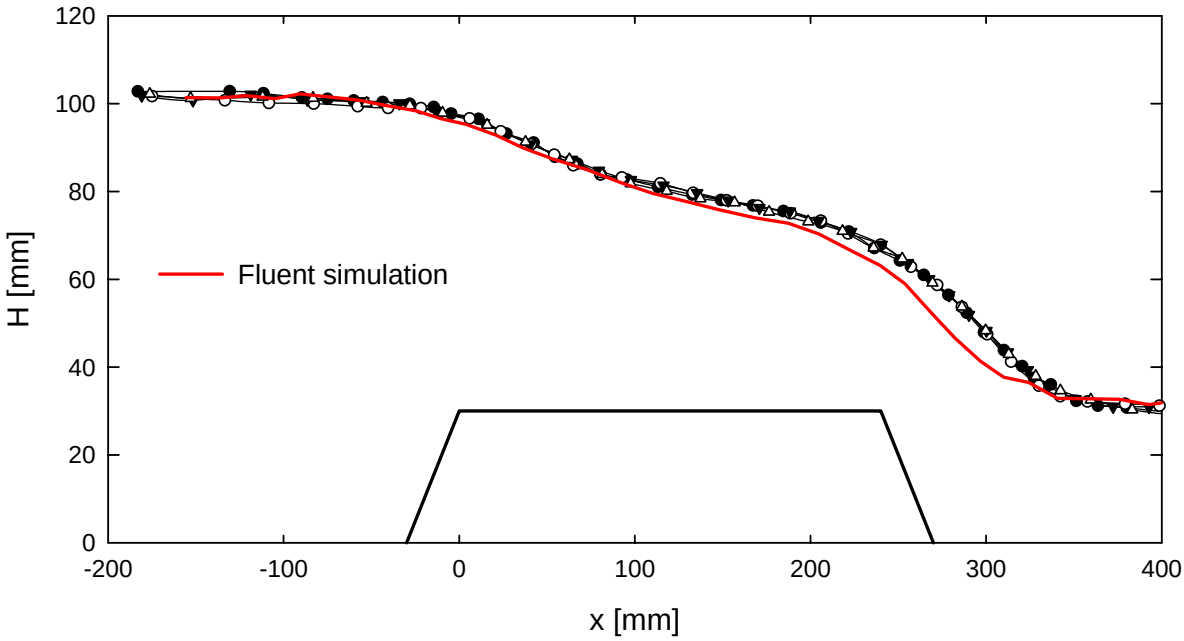

Fig. 5 Free surface profiles over the crest weir – experimental data and CFD modelling (Q=8.7 l/sec)

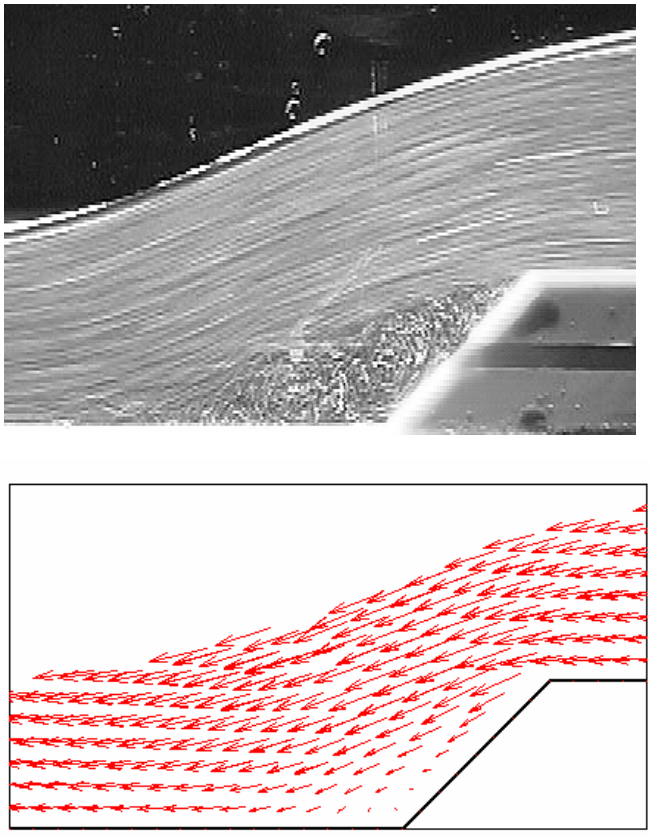

Fig.6 Detail of flow patterns just downstream the weir, upper part – visualization by air bubbles, lower part- result of Fluent calculation

6.2. Unsteady flow condition

To understand the unsteady experiments it is necessary to describe the hydraulic system in more detail. The water is pumped from a tank to the channel by a supply glass pipe of inner diameter 50 mm equipped by the turncock to control the flow rate and the inductive flow meter. The pipe ended in the inlet section below the channel bottom. When the pump is switched off the direction of the flow is reversed and the channel started to drain due to the siphon effect. Therefore the unsteady flow conditions were realised in two steps. In the first the pump was switched off, subsequently the turncock behind the pump was closed to stop the reverse flow. Due to the technical reasons there was some time delay between the pump switching off and closing the valve. The valve closing resulted in an introduction of a shock wave that was propagated back to the channel inlet and resulted in an additional increase of flow depth which was moved along the channel.

Time series of flow rate were used as inputs to the numerical simulation by the Galerkin method. Based on these data the time series of flow depth were calculated. The comparison with experimental observation is shown in Figs. 7 and 8. Local increases of the flow depths are caused by the shock waves initiated by the valve closing. A very good coincidence between the numerical simulations and experimental data was attained for both upstream and downstream positions.

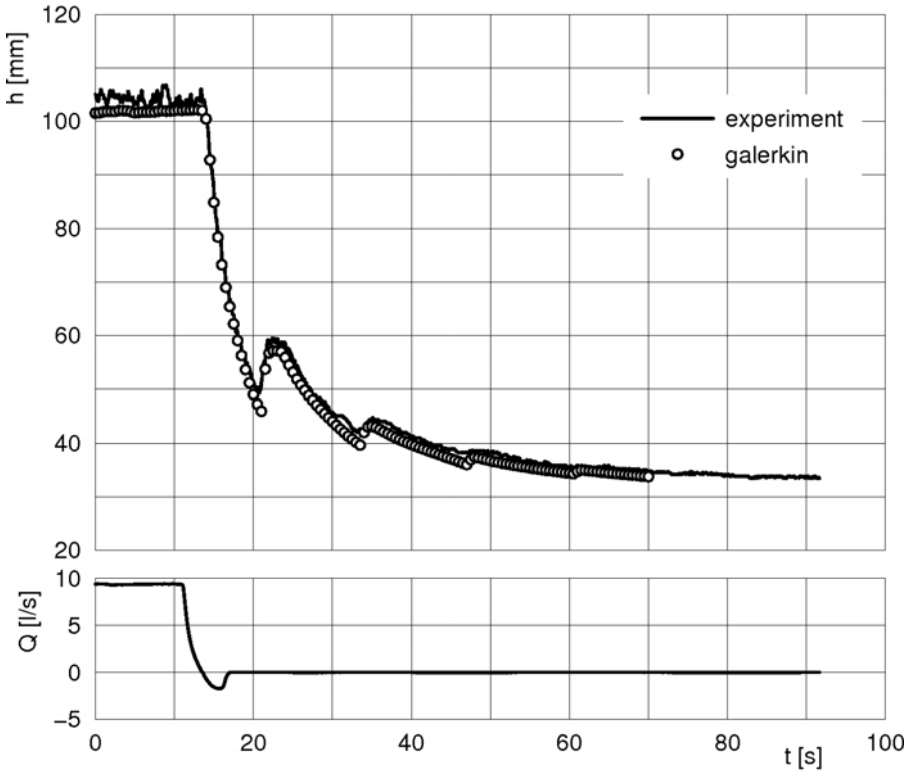

Fig. 7 Time series of free surface and flow rate for unsteady flow condition – upstream position

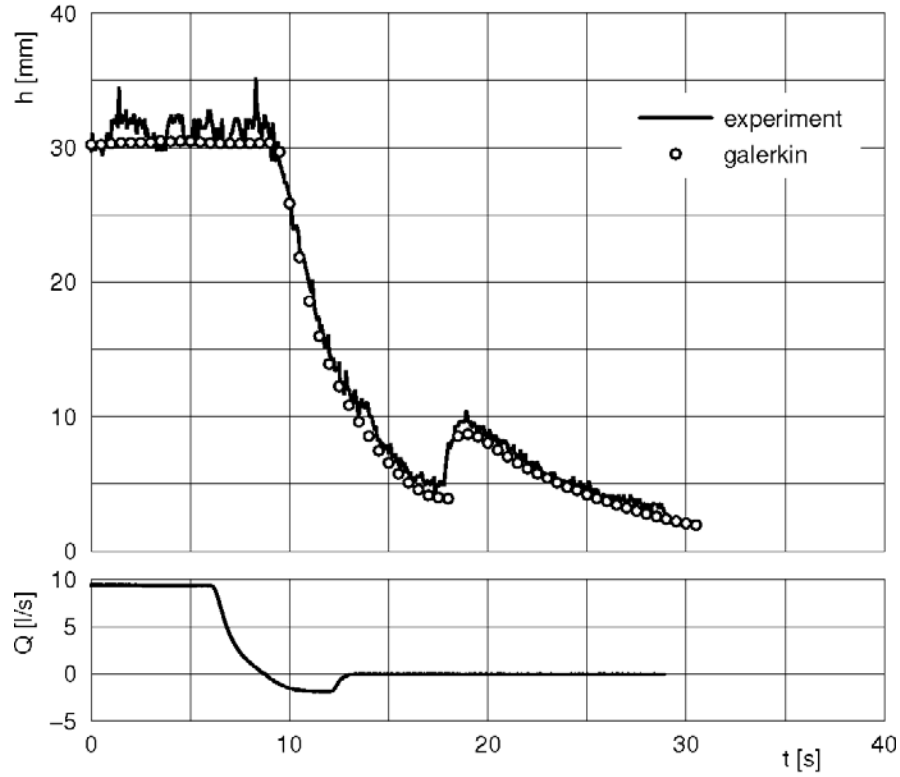

Fig. 8 Time series of free surface and flow rate for unsteady flow condition – downstream position

7. Conclusion

The contribution presents the application of the Glaerkin method solving 1D Shallow Water Equations for both steady and unsteady flow conditions. Due to the neglecting of vertical velocities the numerical solution considerably simplified the flow over obstacles like the broad crest weir. On the other hand the numerical simulation perfectly agrees with real data if the unsteady flow depths are in concern.

8. Acknowledgement

The support under the projects No. 103/03/0724 and 103/04/0970 of Grant Agency of the Czech Republic, and the Institutional Research Plan AV0Z20600510 of ASCR is gratefully acknowledged.

9. References

Atkins, H.L. & Shu, C.W. (1997) Quadrature-free implementation of the discontinuous Galerkin method for hyperbolic equations. *AIAA Journal*, 36(5):775–782.

de Saint-Vennant, A. (1871) Theorie du mouvement non–permanent des eaux, avec application aux cruses des rivieres et a l'introduction des marees dans leur lit. *C.R.Acad.Sc.Paris*, 73:147–154.

Gottlieb, S. & Shu, C.W. (1998) Total variation diminishing Runge–Kutta schemes. *Mathematics of computation*, 67(221):73–85.

Gottlieb, S., Shu, C.W. & Tadmor, E. (2001) Strong stability–preserving high–order time discretization methods. *SIAM Review*, 43(1):89–112.

Hulsen, M.A. (1991) The discontinuous galerkin method with explicit Runge-Kutta time integration for hyperbolic and parabolic systems with source terms. *Technical Report MEMT 19, Delft University of Technology, Laboratory for Aero and Hydrodynamics,* Rotterdamseweg 145, 2628 AL Delft, The Netherlands, November 19.

LeVeque, R.J. (2002) *Finite Volume Methods for Hyperbolic Problems*. Cambridge University Press, Cambridge.

Tseng, M.H. (1999) Verification of 1D transcritical flow model in channels. *Proc.Natl.Sci.Counc.ROC(A)*, 23(5):654–664.